



High dielectric thin films based on UV-reduced graphene oxide and TEMPO-oxidized cellulose nanofibres

Yasir Beeran Pottathara · Vid Bobnar · Yves Grohens · Sabu Thomas · Rupert Kargl · Vanja Kokol

Received: 18 June 2020 / Accepted: 15 January 2021 / Published online: 1 February 2021
© The Author(s), under exclusive licence to Springer Nature B.V. part of Springer Nature 2021

Abstract The dielectric response of thin, flexible films, prepared from graphene oxide (GO) and 2,2,6,6-tetramethylpiperidin-1-yloxy (TEMPO) oxidized cellulose nanofibres (TCNF) is studied using the solution casting method, and further subjected to the UV irradiation treatment under nitrogen atmosphere for GO reduction. The reduction of GO and its interactions with TCNF has been proven by ATR-FTIR, FESEM, UV-Vis, Raman, and XRD spectroscopy measurements. The film's improved storage modules and deformability by temperature are demonstrated by dynamic mechanical analysis. The dielectric constant of the TCGO-3 (contains 3 wt.% GO) composite film

reaches up to 74.05, whereas its 5 h UV treated counterpart even up to 119.2 at a high frequency of 1 MHz. The ac conductivity of the latter film sample reaches $\sim 0.0053 \text{ Sm}^{-1}$. These outstanding dielectric responses of such films indicate their potential to be utilized in energy storage devices, as well as demonstrating their preparation in an environmentally friendly way.

Keywords UV-induced reduction · Cellulose nanofibres · Graphene oxide · TEMPO oxidation · Dielectric properties

Y. B. Pottathara (✉) · R. Kargl · V. Kokol (✉)
Faculty of Mechanical Engineering, University of Maribor, Smetanova Ulica 17, 2000 Maribor, Slovenia
e-mail: yasir.potta@um.si; ptyasirbeeran@gmail.com

V. Kokol
e-mail: vanja.kokol@um.si

V. Bobnar
Condensed Matter Physics Department, Jozef Stefan Institute, Jamova 39, 1000 Ljubljana, Slovenia

Y. Grohens
Univ. Bretagne Sud, IRDL, UMR CNRS 6027, 56100 Lorient, France

S. Thomas
School of Energy Materials and International and Inter-University Centre for Nanoscience and Nanotechnology, Mahatma Gandhi University, Kottayam 686560, India

Introduction

Research and development on green renewable materials have attained extensive attention recently due to their peculiar properties, such as biodegradability, recyclability, low cost, and lightweight nature (Gopi et al. 2019). Particularly, cellulose nanofibrils (CNFs), also possessing significant physical and chemical properties (high mechanical strength and crystallinity, low density, high specific surface area, and abundance of hydroxyl groups (Klemm et al. 2011; Isogai and Bergström 2018; Li et al. 2018)), have been shown as an ideal material for producing flexible films with functional characteristics such as electrical conductivity and energy storage properties (Shi et al. 2014; Yang et al. 2015; Zhang et al. 2019; Zhao et al. 2019).

Such features have, thus, been utilized broadly in flexible electronics (Jung et al. 2015; Yin et al. 2020), supercapacitors (Yang and Li 2015), energy storage gadgets (Lay et al. 2017), electromagnetic interference (EMI) shielding materials (Gopakumar et al. 2018), triboelectric nanogenerators (Shi et al. 2020), sensors (Koshy et al. 2017), solar cells (Yuwawech et al. 2015), and thermal insulations (Hasan et al. 2019).

Recently, nanocellulose based flexible dielectric energy storage composites have been widely reported in modern electronic devices (Poyraz et al. 2017; Yang et al. 2018; Tao et al. 2019; Tao and Cao 2020). The CNF films prepared with polyaniline (Gopakumar et al. 2018), barium titanate (BaTiO_3) (Tao et al. 2020), titanium dioxide (TiO_2) (Tao et al. 2019), multi-walled carbon nanotubes (MWCNT) (Tao and Cao 2020), silica and polyvinyl alcohol (PVA) (Poyraz et al. 2017), and graphene (Beeran et al. 2016; Pottathara et al. 2018, 2019b), thus showing improved dielectric properties at a different frequency range from 1 kHz up to 10 MHz (Poyraz et al. 2017). The composite films of CNF/ TiO_2 showed a relative dielectric constant of 19.51 at 1 kHz with a loading of 50 wt.% of TiO_2 (Tao et al. 2019). At 1 kHz, flexible dielectric films of CNF incorporated with 6.2 wt.% of acid oxidized MWCNT showed a dielectric constant of 73.88 and an AC conductivity of $1.77 \times 10^{-7} \text{ S cm}^{-1}$ (Tao and Cao 2020). The lower dielectric loss values of transparent films from TEMPO-oxidized CNF incorporated with Eu are also described as flexible dielectric energy materials (Yang et al. 2018). More significant enhancement on dielectric properties, a dielectric constant of 52 and an AC conductivity of $3.46 \times 10^{-4} \text{ S cm}^{-1}$ at a higher frequency of 1 MHz, was previously reported by our group with ammonia functionalized graphene oxide (GO) reinforced TCNF flexible films (Beeran et al. 2016). Generally, the TCNF offers huge specific surface areas of about $800 \text{ m}^2 \text{ g}^{-1}$ (Isogai and Bergström 2018), with an abundance of carboxylate groups and a tensile strength of about 3 GPa (Saito et al. 2013), thus showing a better alternative to pristine CNF. This is related to the presence of an intensive amount of charges which makes water suspended TCNF highly favourable for nano-dispersibility and hydrocolloidal stability of different nanomaterials, including inorganic fillers, as well as matrix materials for functional device fabrication.

We have shown that the dielectric properties of GO incorporated into CNF composites can also be achieved by in-situ UV induced reduction of GO (Pottathara et al. 2019b). In the present work, the effect of time-related UV-induced reduction of GO embedded into the TCNF-based films, are thus studied by different spectroscopy techniques and potentiometric charge titration. The morphological structure, dynamic mechanical analysis, and dielectric properties are analysed thoroughly for evaluating their dielectric and mechanical storage properties.

Experimental

Materials

Cellulose nanofibres (CNFs) as acquired from the University of Maine, USA. Chemicals for preparation of graphene oxide (GO) and TEMPO oxidation of CNF, such as graphite flakes, NaNO_3 , H_2SO_4 , H_2O_2 , KMnO_4 , NaClO , (2,2,6,6-tetramethylpiperidin-1-yl) oxyl (TEMPO), and NaBr , were procured from Sigma-Aldrich, Slovenia.

Oxidization of CNF using the TEMPO reagent

The oxidization of CNF was done by using the TEMPO reagent based on the previous reports (Saito et al. 2006, 2007; Pottathara et al. 2019a, b). First, the TEMPO reagent (0.0147 g) and NaBr (0.162 g) were dissolved in water and added up to the CNF dispersion (1 wt.%), and then 25 mL of 10% NaClO solution was added slowly to this solution. The final solution's pH was controlled by 0.1 M of NaOH and HCl , and remained constant for 3 h. The final product was quenched with 7 mL of ethanol and washed thoroughly. By potentiometric charge titration, the carboxylate content has been estimated for TCNF samples to be $1.63 \pm 0.21 \text{ mmol/g}$ against $0.3 \pm 0.15 \text{ mmol/g}$ for pristine CNF (Beeran et al. 2016).

Synthesis of graphene oxide (GO)

The previously reported Hummers method (Hummers and Offeman 1958; Marcano et al. 2010) was utilized for GO preparation. Here, 24 mL of conc. H_2SO_4 was added to a mixture of graphite flakes (1 g) and NaNO_3

(0.5 g) and then cooled to 0 °C. To this mixture, 3 g of KMnO_4 was added slowly under a monitored temperature of lower than 20 °C. Later, this mixture was warmed up to a temperature of 35 °C and stirred for 90 minutes. Next, about 46 mL of warm water was added slowly to this mixture. Later, the temperature of the solution could be raised up to 98 °C and then further diluted with 132 mL of warm water, and finally treated with 3% of H_2O_2 . The final solution was washed and centrifuged several times, and, finally, GO powder was obtained as a solid yellow-brown powder after drying the resultant suspension.

Fabrication of TCNF-GO composite films

The composite films of TCGO were manufactured by solution casting of TCNF-GO dispersions. Homogeneous dispersions of GO were prepared with the mixing of GO (200 mg) in 100 mL of deionized water for 60 minutes by an ultrasonication processor (CV 334, Sonics, USA). Later, GO dispersions with 0.003 g, 0.006 g, 0.0125 g, and 0.019 g of GO were blended with TCNF (50 mL, 1.2 wt.%) employing a magnetic stirrer (Tehtnica Rotamix SHP-10, Slovenia) for 30 minutes. The TCNF-GO dispersions of 20 mL were finally cast into Petri dishes of 50 mm diameter and dried at room temperature. The resultant composite films were marked as TCGO-0.5, TCGO-1 TCGO-2, and TCGO-3 regarding the amount (wt.%) of GO in the prepared films. Reference films without the GO content were made, named as TCNF.

UV-irradiation experiment

A Digital UV ozone system, (Novascan, USA) was employed to perform the UV-irradiation experiments, as shown in Fig. 1. The UV chamber was equipped with a 300 W mercury vapour lamp without filter and allowed to dry under nitrogen atmosphere. The composite film samples were kept at 10 cm distance from the UV lamp, and the samples were irradiated systematically for 0.5 h, 1 h, 2 h, and 5 h to verify their capability for UV treatments.

Characterization

FESEM (Ultra Plus, Zeiss, Germany), imaging was performed to examine the morphology of the films before and after UV irradiation. An ion sputter System

(Gatan-682, USA) was used for coating a Pt layer on the samples.

A Lambda 900 (Perkin Elmer UK) UV–Vis spectrophotometer was employed to record the transmittance of film samples. The spectra were recorded at wavelengths in between 250 and 750 nm with 450 nm min^{-1} of scanning speed.

Potentiometric charge titration was employed to quantify the carboxyl content in the composites before and after UV treatment. The instrument (Mettler Toledo T70, Switzerland) equipped with a two-burette system, including a Mettler TDG 117 glass electrode, was employed for the measurements. The two-burette system was filled with 0.1 M HCl and 0.1 M KOH. The titrations were conducted in an N_2 -gas atmosphere at room temperature, and the carboxylic content was calculated from back-titration data.

ATR-FTIR spectra were recorded by using an IR spectrophotometer (Perkin Elmer UK) between 4000 and 500 cm^{-1} at 4 cm^{-1} resolutions from 16 scans. An air spectrum was used as the background. The Spectrum 5.0.2 Software program was utilized for the data acquisition analysis.

A Bruker D8 diffractometer (Germany) was used to record the X-ray Diffraction (XRD) pattern of the composite films. The XRD patterns were recorded from 5° to 55° (2 θ value) with 2° min^{-1} of scan rate with operating voltage and current of 40 kV a 40 mA respectively at 23 ± 1 °C using Cu $\text{K}\alpha$ radiation.

A Horiba LabRAM Raman spectrometer (Germany) having an Ar-ion laser with the excitation wavelength of 514 nm was employed to record the Raman spectra.

The dynamic mechanical analysis (DMA) was performed with a Perkin Elmer DMA 8000, using rectangular-shaped samples (5 × 2.5 × 0.55 mm³) at a heating rate of 4 °C / min up to 250 °C with a frequency of 10 Hz.

Cr/Au sputtered film samples with a 0.4 mm diameter were used for dielectric studies. A Novocontrol Alpha High-Resolution Dielectric Analyser (Novocontrol Technologies GmbH, Hundsangen, Germany) was employed to estimate the capacitance, C, and conductivity, G, within the frequency range of 10 Hz–1MHz. The amplitude of the probing AC electric signal was set as 50 mV. The dielectric permittivity, ϵ' , and AC electrical conductivity, σ' , were estimated by using the equations, $\epsilon' = (\text{Cd})/(\epsilon_0\text{S})$ and $\sigma' = \text{Gd/S}$. Here, 'S' implied the electrode's area

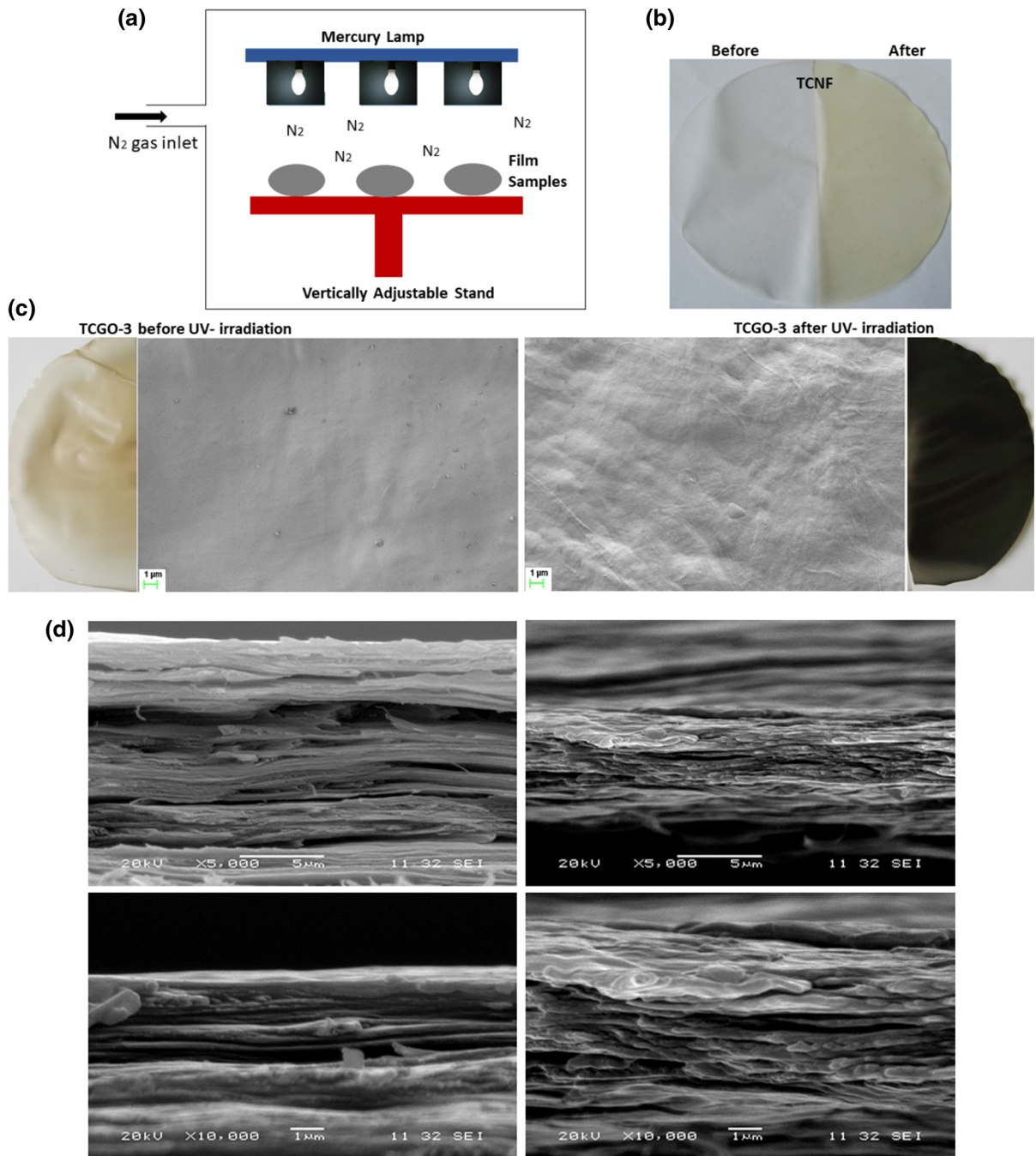


Fig. 1 Set up for UV-irradiation experiments (a), Digital and FE-SEM images of TCNF and TCGO-3 films before and after UV irradiation experiment (b) and (c), FE-SEM cross-sectional

images with different magnification for TCGO-3 films before (left) and after (right) UV irradiation experiment (d)

and ‘d’ implied the film’s thickness, whereas ϵ_0 indicated the dielectric constant of free space.

Results and discussion

The effect of UV irradiation on the films’ physicochemical and morphological properties

Figure 1a shows the UV-irradiation experimental set-up and Fig. 1b the digital images of pristine TCNF films before and after UV treatment. The white-coloured and homogeneous pristine TCNF films transformed into a yellowish, but stable, film after the UV treatment. The reduction of GO by UV treatment was also confirmed optically by the colour changes of the films from light yellowish to black (Fig. 1c). In addition, FE-SEM images (Fig. 1c) reveal the changes in the films’ surface morphology after UV treatment, being reflected in a rough surface, denser and more packed structure compared to the untreated samples. Figure 1.

D shows the cross-sectional FESEM images of TCGO-3 films before and after UV irradiation. The successful addition of GO and its good reinforcement capability in the TCNF matrix is exemplified by the smoothness in the images [27]. The compactly stacked structure of films was changed to a rougher orientation but maintaining a continuous layered network after the UV treatment. The effect of reduction is also reflected in a noticeable decrease of transmittance spectra (Fig. 2) for the film samples, measured in a region of 250–750 nm. The transparency of UV treated reference films decreased already at the reference samples

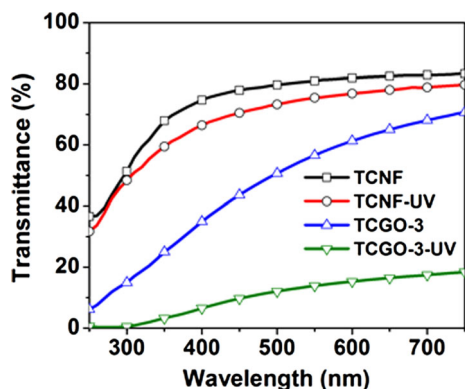


Fig. 2 UV-Vis spectra for untreated TCNF and TCGO-3 films compared with their 5 h of UV treated counterparts

(without GO content), is further reflected in the lowest transmittance values of about 18% for the UV-treated TCGO-3 film sample in comparison with the untreated film given transmittance of about 71% at 750 nm.

Further spectroscopic analysis was performed to understand the changes of both TCNF and GO structure and their interactions after the UV treatment. The pristine TCNF films and their nanocomposites with different amounts of GO (Fig. 3a) in addition to UV treated TCGO-3 film samples (Fig. 3b) were investigated by ATR-FTIR. The pristine TCNF film shows typical cellulose associated IR bands at $\sim 1023\text{ cm}^{-1}$, $\sim 1028\text{ cm}^{-1}$, $\sim 1160\text{ cm}^{-1}$, $\sim 1318\text{ cm}^{-1}$, $\sim 2900\text{--}2923\text{ cm}^{-1}$, $\sim 3333\text{--}3335\text{ cm}^{-1}$, plus a band at $\sim 1596\text{ cm}^{-1}$ corresponding to the carboxylate ions (COO^-), and a small band at $\sim 1739\text{ cm}^{-1}$ for the protonated carboxylic acid groups (Beeran et al. 2016). Besides, the peak positioned about $\sim 1023\text{--}1028\text{ cm}^{-1}$ is typical for the C–O stretching vibration of anhydrous groups, and the vibration peak positioned at $\sim 1318\text{ cm}^{-1}$ implies the bending vibrations of C–H bonds in the cellulose glucose rings (Beeran et al. 2016). The TCGO films show the spectrum with similar adsorption bands as for pristine TCNF, while fast reduction in intensities for the C=O stretching vibration peak positioned at $\sim 1596\text{ cm}^{-1}$, as well as the intensity of the stretching vibration of -CH₂ peaks at about 2850 cm^{-1} and OH related region, can be observed for the UV-irradiated TCGO samples, implying strong interactions between the GO and cellulosic fibrils.

To check the effect of UV treatment on the films’ structure more systematically, ATR-FTIR spectra of TCNF and TCGO-3 film samples were deconvoluted (Fig. 4) at relevant spectral regions, i.e., in the C=O range between $1500\text{ and }1800\text{ cm}^{-1}$ and in the OH region between $3000\text{ and }3700\text{ cm}^{-1}$, before and after UV irradiation. Unseen peaks were observed in the deconvoluted spectral lines between $3000\text{ and }3700\text{ cm}^{-1}$ for both TCNF and TCGO, which is related to specific inter- and intramolecular vibrations, i.e., the O–H stretching was denoted as the first peak, the inter-molecular hydrogen bond of O(6)H–O as the second and third peaks, whereas the intra-molecular hydrogen bond of O(3)H–O was denoted as the fourth and fifth peaks, and the sixth peak was assigned as the intra-molecular hydrogen bond of O(2)H–O (Beeran et al. 2016). The UV irradiated TCNF sample reveals a two-fold reduction of peaks related to the aromatic

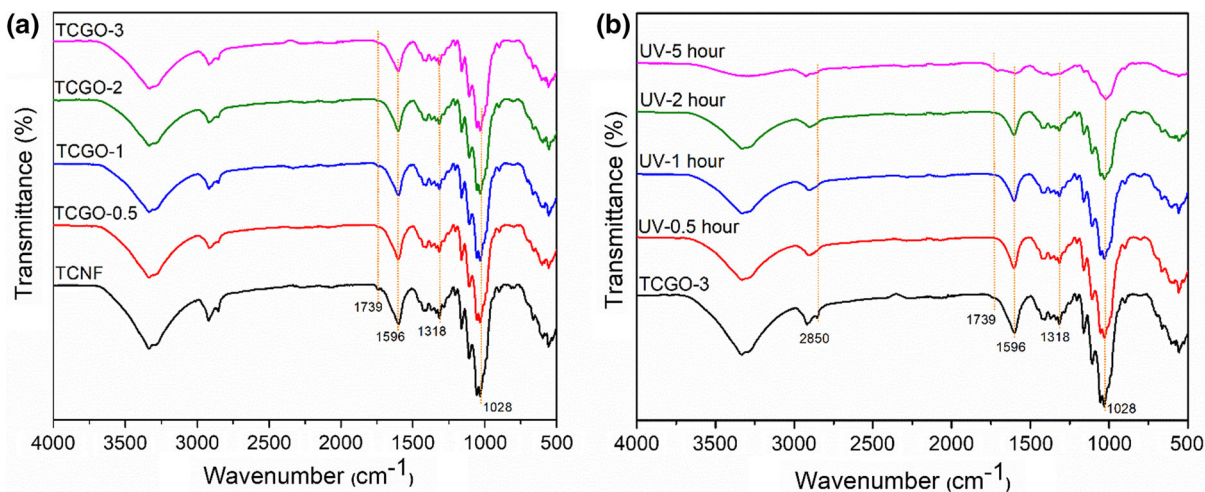


Fig. 3 ATR-FTIR spectra of **a** Pristine TCNF and its composites with 0.5, 1, 2, and 3 wt.% of GO, and **b** TCGO-3 film, with and without 0.5, 1, 2 and 5 h of UV-treatment

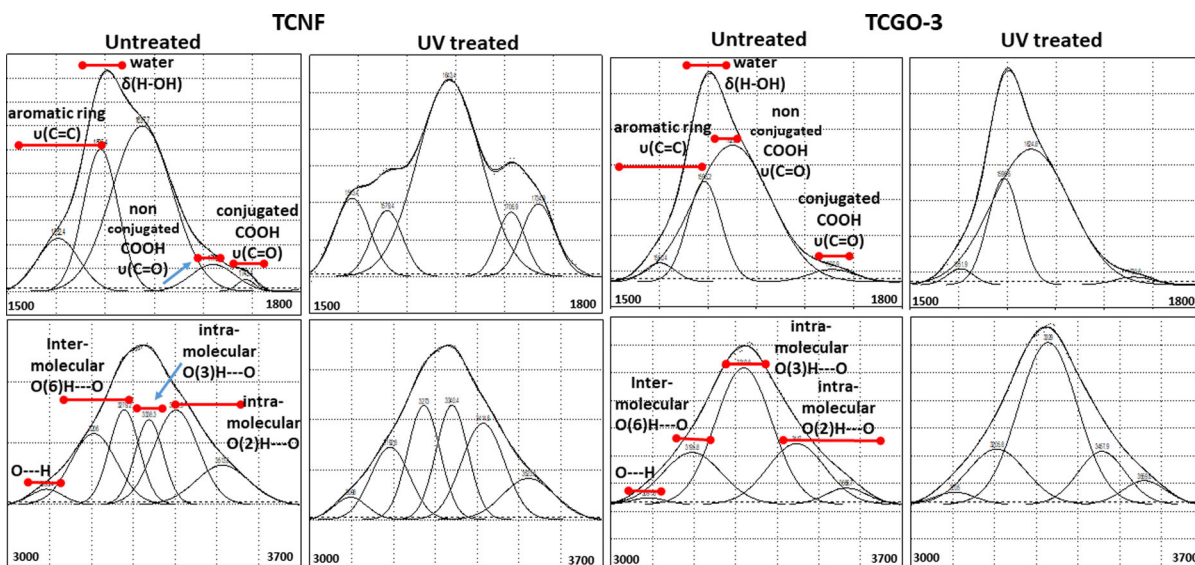


Fig. 4 De-convoluted ATR-FTIR spectra in the C=O range (between 1500–1800 cm^{-1}) and the OH region (between 3000–3700 cm^{-1}) of untreated and UV treated (5 h) TCGO-3 film samples

ring, being accompanied with an increase of (non)-conjugated COOH groups in the C=O related vibrations area without changing the OH related region, which may also indicate some degradation of the glucose rings during UV treatment. The GO addition in the TCNF matrix results in the dominance of intra-molecular bonding with O(3)H, while inter-molecular bonding stayed almost the same, which may be attributed to the quantitatively small amounts of residual and sterically available O(6)H groups, which

did not change after UV irradiation. On the other hand, a smaller and broader non-conjugated COOH band is observed in the C=O related region, which didn't change after 5 h of the UV irradiated TCGO sample, despite the simultaneous reduction of GO, which shall yield additional COOH groups. These observations can be related to graphene reduction, as already described in previous reports (Nyangiwe et al. 2015).

Figure 5a gives evidence about the changes in the crystalline structure of CNF, as well as GO after the

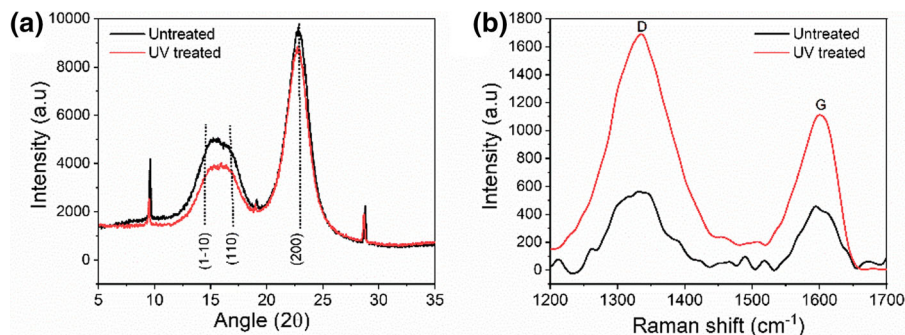


Fig. 5 **a** XRD spectra and **b** Raman spectra for untreated and UV treated (5 h) TCGO-3 film samples

UV treatment. The partial crystalline nature of cellulose was revealed by the broad diffraction peak positioned at 16° (Nishiyama et al. 2009) and a peak placed at 22° , corresponding to the (110) and (200) crystalline planes respectively, typical for cellulose I allomorph (French 2014). The presence of an intense peak at 9° corresponds to the crystalline reflection of GO particles. For the UV treated TCGO sample, the substantial reduction of intensity for GO related and TCNF amorphous phase related peaks, compared to the untreated sample, confirmed the reduction of GO, as well as reducing the amorphous phase of TCNF after the UV treatment. The Raman spectra (Fig. 5b) confirm the reduction of GO by an increase, and the ratio of intensities for its D and G bands (Jorio et al. 2011) from 1.24 to 1.52 for the UV treated sample, compared to the untreated sample. This increment can be attributed to the elimination of oxygen during the reduction. It also suggests the creation of new graphitic domains, along with the increased sp^2 cluster number (Ferrari and Robertson 2000).

The schematic illustration of the mechanism of the reduction of GO and CNF under UV irradiation and its interactions are presented in Fig. 6. It is reported that UV irradiation activates the photolytic chain splitting of cellulose molecules, ensuing free radicals' formation (Kleinert 1964). The radical reactions upon UV light would lead to dehydration and decarboxylation of composite materials. The removal of functional moieties such as the carboxyls/carbonyls can lead to the reduction of the bonding mode of cyclic/aliphatic compounds that results in the reduction of GO (Pei and Cheng 2012). The effective removal of attached functional moieties on the GO sheets, as well as the increased interaction (strong hydrogen bonding) with TCNFs, were already detected by the previous studies (Beeran et al. 2016). During the UV irradiation process, the oxidized volatile species or reduced groups are supposed to be responsible for the reduction of GO in TCNF composites.

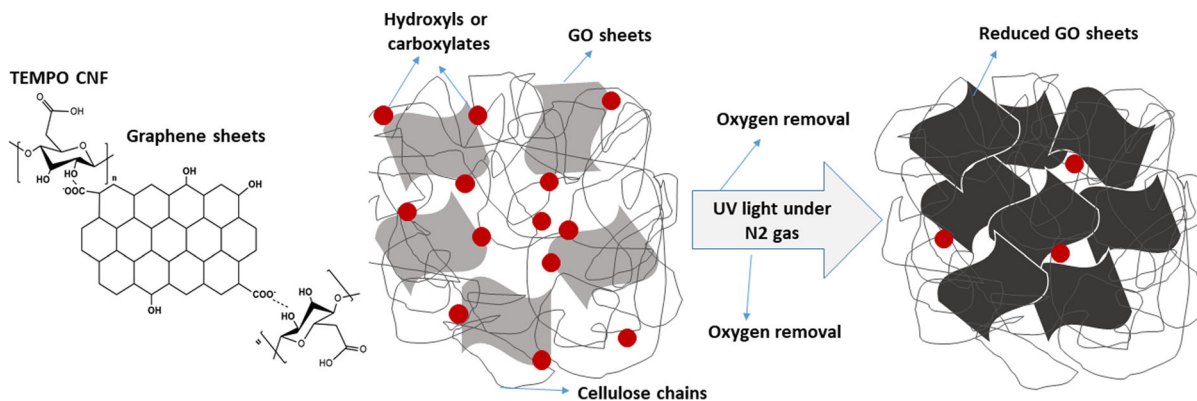


Fig. 6 Schematic illustration of the mechanism for GO and CNF reduction under UV irradiation and its interactions

Temperature-dependent dynamic mechanical properties

The dynamic mechanical analysis was executed to evaluate variations in mechanical properties between 25 and 180 °C for untreated and 5 h UV treated TCGO-3 film samples (Fig. 6). Generally, the dynamic mechanical analysis evaluates the sample's responses to the applied oscillatory stress. At 25 °C, TCGO-3 has a mechanical storage modulus value of about 25.9 GPa, whereas the UV irradiation improves it substantially to about 30.1 GPa, which may be related to the free radical cross-linking mechanism that increases the film density as already reported in our previous study (Pottathara et al. 2019b). The storage modulus decreases with an increase in temperature. This decrement is sudden until around 70 °C, and then the slope is showing a steady trend for the remaining temperature region. The increment of retention ratio, the ratio of E1 at 150 °C to that at 25 °C, with the UV treatment, attains the maximum value of 0.79, implying a higher influence of heat on the deformability. Moreover, at higher temperatures (> 160 °C), the composite film cracked and the analysis was stopped, demonstrating the high temperature sensitivity of such a film (Beeran et al. 2016). The results prove, however, that the examined film samples can be utilized in energy storage devices up to 160 °C upon recharging (Zhang et al. 2007) (Fig. 7).

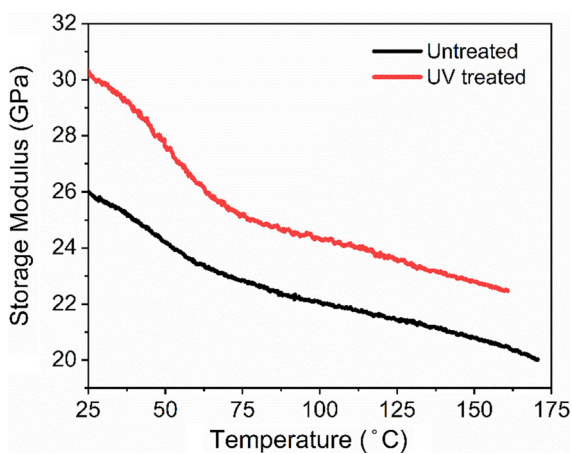


Fig. 7 The changing of dynamic storage modulus as the function of temperature (a) and time (b) for untreated and UV treated (5 h) TCGO-3 film sample

Frequency dependent dielectric properties of UV treated films

The dielectric response of TCGO composite films with various GO weight fractions are shown in Fig. 8. The dielectric constant increases with frequency-lowering, which is a very common behaviour—it could be due either to the contribution of space charges or due to the external impacts, such as the existence of surface layers (Lunkenheimer et al. 2002). Over the entire frequency range, the films' dielectric constant, ϵ' , improved steadily with respect to the addition of GO. A similar trend was observed for most of the former reports of graphene incorporated polymer composites (Wu et al. 2013; Liao et al. 2014; Kafy et al. 2015b; Ning et al. 2015; Tong et al. 2015).

In the last decade, various composites were reported with graphene-based fillers in cellulosic matrices. For graphene-filled cellulose composites, the dielectric values in the present study show significant enhancement to previous reports (Kafy et al. 2015a, b, 2016; Wang et al. 2018; Gnidakoung et al. 2019), and the comparison is depicted in Table 1. Recently, Wang et al. (2018) demonstrated rGO filled cyanoethyl cellulose nanocomposite films with a dielectric constant of 472 (for 9.7% rGO) at a frequency of 1 kHz. The intrinsic materials' properties are usually provided at higher frequencies, where the response is not governed by space charge contribution. In the present study, TCGO-3 composite films have a very high dielectric constant of 74.05, even at the frequency of 1 MHz (see Fig. 8a). This enhancement is most probably the result of the interface polarisation. Namely, according to the Maxwell-Wagner-Sillars effect, in the case of nanocomposites, charges will accumulate at the interface between the polymer matrix and the filler (Yuan et al. 2011). Numerous micro-capacitor networks will be formed in the composites, with graphene sheets acting as electrodes and cellulose matrices acting as a dielectric. Moreover, the improved dielectric properties (compared to all previous reports) can, in our samples, be due to the interfacial bonding between GO and the cellulosic matrices by hydrogen bonds, due to the improved dispersion effect. A similar tendency was noticed in the ac conductivity, σ' , (Fig. 8b), which was increasing with the amount of GO fillers. At 1 MHz, the TCGO-3 film shows an ac conductivity of $\sim 0.0014 \text{ S m}^{-1}$. Finally, a higher amount of carboxylic groups

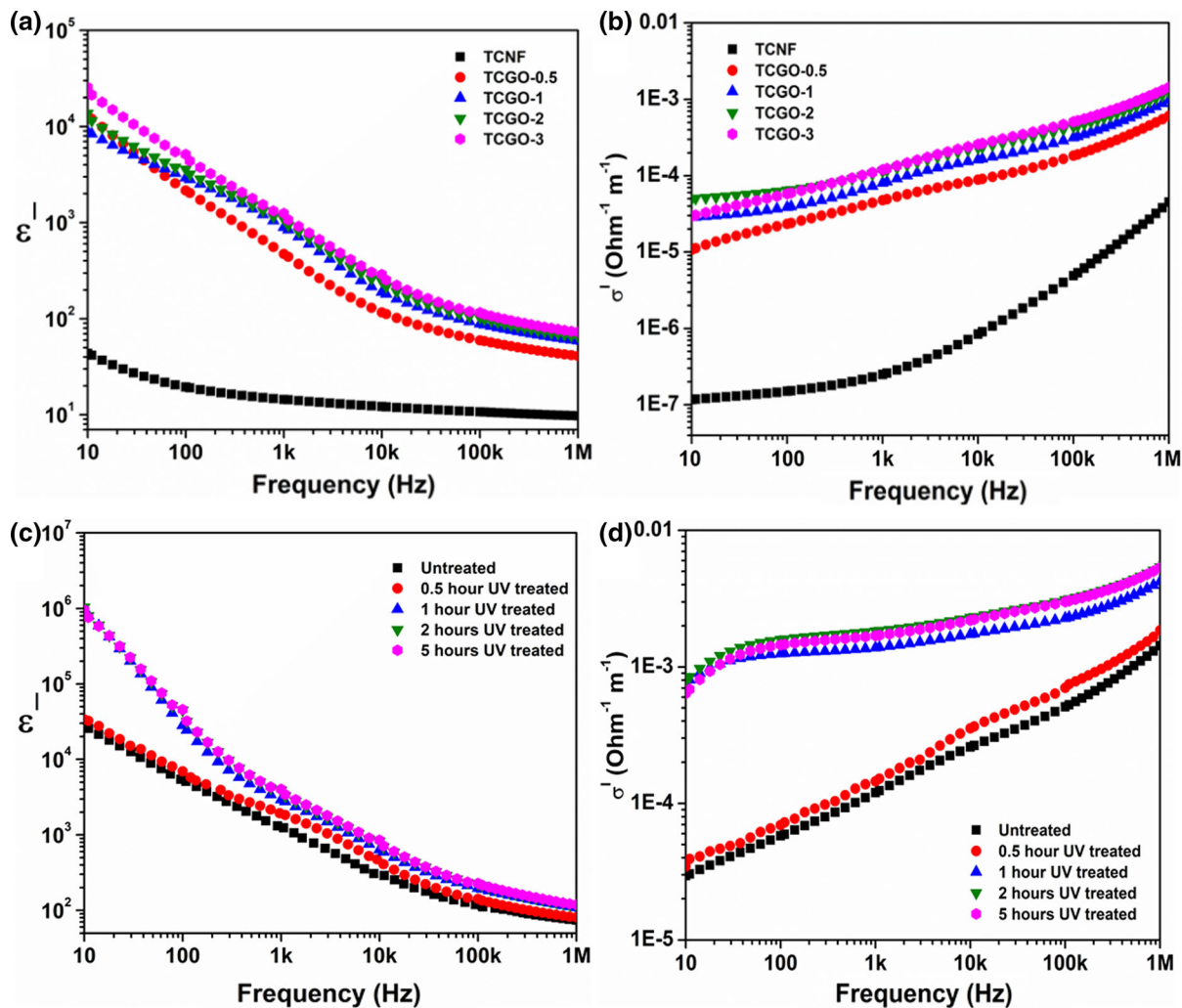


Fig. 8 The dielectric constant ϵ' (a, c) and ac conductivity σ' (b, d) with respect to frequency for untreated and UV treated TCGO films measured at room temperature

content in TCNF and, thus, more trapped charges at the interface in the case of TCGO composites, may also be responsible for the relatively high ϵ' and values σ' of the present samples.

Figure 8c and d present ϵ' and σ' values of TCGO-3 composite films after different UV treatment times. All samples show an increase of ϵ' and σ' with respect to longer UV-irradiation time. At 1 MHz, the 5 h UV treated TCGO-3 film shows ϵ' of 119.2 and σ' of $\sim 0.0053 \text{ S m}^{-1}$. In contrast to untreated samples, the reduction of graphene oxide offers more MWS polarisation sites in the composites, which leads to improved dielectric properties (Pottathara et al. 2019b). The UV treatment stimulated reduction of

GO and, therefore, decreased the distance between graphene flakes which indicates a high capacitance. This can be supported by decreasing of films thickness (cross-section), according to the SEM images provided in Fig. 1d, and, therefore, an increase of the density of films causing a decreased distance of the graphitic sheets. However, a part of the thickness decrease will also be caused by mass loss during UV treatment. Furthermore, after the reduction, because of the oxygen removal, higher intrinsic conductivity of graphitic sheets will be considered and ac conductivity increases.

Table 1 Comparison of dielectric constants at different frequencies for various cellulose based composites

Cellulose derivatives	Filler material	Filler conc. (wt.%)	Dielectric constant at					Refs.
			20 Hz	50 Hz	1 kHz	10 kHz	1 MHz	
Cyanoethyl cellulose	rGO	9.7			472			Wang et al. (2018)
CNF	Barium titanate	30			188.03			Tao et al. (2020)
Cellulose acetate	Modified rGO	1				9.8		Mohiuddin et al. (2015)
Cellulose acetate	Al ₂ O ₃	25		27.57				Deshmukh et al. (2017)
Cellulose nanocrystal	GO	10	3857					Kafy et al. (2016)
Cellulose	GO	1	1052					Kafy et al. (2015b)
Cyanoethylatedcellulose	Montmorillonite	5			71			Madusanka et al. (2017)
Cellulose	rGO				100			Sadasivuni et al. (2015)
CNF	Carbon nanotubes	4.5			3198			Zeng et al. (2016)
CNF	Ammonia functionalised GO	3					46.1	Beeran et al. (2016)
TEMPO-CNF	Ammonia functionalised GO	3					51.4	Beeran et al. (2016)
CNF	GO	3					68.92	Pottathara et al. (2019b)
TEMPO-CNF	GO	3					74.05	Present work
TEMPO-CNF	UV irradiated GO	3					119.2	Present work

Conclusions

The structural, mechanical, and dielectric responses were studied of UV-irradiated graphene oxide (GO) incorporated TEMPO-oxidized cellulose nanofibres (TCNF) self-standing composite films (TCGO). The reduction of GO in the TCNF matrix was confirmed by the colour change, resulting in mechanically stable films up to 160 °C, and an increased mechanical storage modulus as the result of the free radical cross-linking mechanism given much higher dielectric responses (ϵ' of 119.2 and σ' of $\sim 0.0053 \text{ S m}^{-1}$) at a frequency of 1 MHz, comparable to that found in the existing literature. The results confirm that composite films can be utilized in energy storage devices to survive higher temperatures upon recharging, as well as showing their potential in high dielectric storage applications. Moreover, this environmentally benign method of GO reduction by UV irradiation offers a substitute against harmful chemical processes, which can be extendable to other nanocomposite biomaterials.

Acknowledgements The authors are grateful to the Erasmus Mundus Euphrates (2013–2540/001-001-EMA2) for financial support.

Funding Erasmus Mundus Euphrates (2013-2540/001-001-EMA2).

Compliance with ethical standards

Conflict of interest The authors declare that they have no conflicts of interest to reveal.

References

- Beeran Y, Bobnar V, Gorgieva S, Grohens Y, Finšgar M, Thomas S, Kokol V (2016) Mechanically strong, flexible and thermally stable graphene oxide/nanocellulosic films with enhanced dielectric properties. *RSC Adv* 6(54):49138–49149. <https://doi.org/10.1039/C6RA06744A>
- Deshmukh K, Ahamed MB, Deshmukh RR, Pasha SK, Sadasivuni KK, Polu AR, Ponnamma D, AIMaadeed MA, Chidambaram K (2017) Newly developed biodegradable polymer nanocomposites of cellulose acetate and Al₂O₃ nanoparticles with enhanced dielectric performance for embedded passive applications. *J Mater Sci Mater Electron* 28(1):973–986. <https://doi.org/10.1007/s10854-016-5616-9>
- Ferrari A, Robertson J (2000) Interpretation of Raman spectra of disordered and amorphous carbon. *Phys Rev B Condens Matter Mater Phys* 61(20):14095. <https://doi.org/10.1103/PhysRevB.61.14095>
- French AD (2014) Idealized powder diffraction patterns for cellulose polymorphs. *Cellulose* 21(2):885–896. <https://doi.org/10.1007/s10570-013-0030-4>

- Gnidakoung JRN, Gao X, Kafy A, Kim J, Kim JH (2019) Fabrication and electrical properties of regenerated cellulose-loaded exfoliated graphene nanoplatelet composites. *Carbon Lett* 29(2):115–122. <https://doi.org/10.1007/s42823-019-00003-5>
- Gopakumar DA, Pai AR, Pottathara YB, Pasquini D, Carlos de Moraes L, Luke M, Kalarikkal N, Grohens Y, Thomas S (2018) Cellulose nanofiber-based polyaniline flexible papers as sustainable microwave absorbers in the X-band. *ACS Appl Mater Interfaces* 10(23):20032–20043. <https://doi.org/10.1021/acsami.8b04549>
- Gopi S, Balakrishnan P, Chandradhara D, Poovathankandy D, Thomas S (2019) General scenarios of cellulose and its use in the biomedical field. *Mater Today Chem* 13:59–78. <https://doi.org/10.1016/j.mtchem.2019.04.012>
- Hasan M, Gopakumar DA, Arumughan V, Pottathara YB, KS S, Pasquini D, Bračić M, Seantier B, Nzihou A, Thomas S, Rizal S, HPS AK (2019) Robust superhydrophobic cellulose nanofiber aerogel for multifunctional environmental applications. *Polymers* 11(3):495. <https://doi.org/10.3390/polym11030495>
- Hummers WS, Offeman RE (1958) Preparation of graphitic oxide. *J Am Chem Soc* 80(6):1339. <https://doi.org/10.1021/ja01539a017>
- Isogai A, Bergström L (2018) Preparation of cellulose nanofibers using green and sustainable chemistry. *Curr Opin Green Sustain Chem* 12:15–21. <https://doi.org/10.1016/j.cogsc.2018.04.008>
- Jorio A, Dresselhaus MS, Saito R, Dresselhaus G (2011) Raman spectroscopy in graphene related systems. Wiley, New York
- Jung YH, Chang TH, Zhang H, Yao C, Zheng Q, Yang VW, Mi H, Kim M, Cho SJ, Park DW, Jiang H (2015) High-performance green flexible electronics based on biodegradable cellulose nanofibril paper. *Nat Commun* 6(1):1–11. <https://doi.org/10.1038/ncomms8170>
- Kafy A, Sadasivuni KK, Akther A, Min SK, Kim J (2015a) Cellulose/graphene nanocomposite as multifunctional electronic and solvent sensor material. *Mater Lett* 159:20–23. <https://doi.org/10.1016/j.matlet.2015a.05.102>
- Kafy A, Sadasivuni KK, Kim HC, Akther A, Kim J (2015b) Designing flexible energy and memory storage materials using cellulose modified graphene oxide nanocomposites. *Phys Chem Chem Phys* 17:5923–5931. <https://doi.org/10.1039/C4CP05921B><https://doi.org/>
- Kafy A, Akther A, Shishir MIR, Kim HC, Yun Y, Kim J (2016) Cellulose nanocrystal/graphene oxide composite film as humidity sensor. *Sens Actuators A Phys* 247:221–226. <https://doi.org/10.1016/j.sna.2016.05.045>
- Kleinert TN (1964) Free radical reactions in UV irradiation of cellulose. *Holzforschung Int J Biol Chem Phys Technol Wood* 18(1–2):24–28. <https://doi.org/10.1515/hfsg.1964.18.1-2.24>
- Klemm D, Kramer F, Moritz S, Lindström T, Ankerfors M, Gray D, Dorris A (2011) Nanocelluloses: a new family of nature-based materials. *Angew Chem Int Ed* 50(24):5438–5466. <https://doi.org/10.1002/anie.2011001273>
- Koshy O, Pottathara YB, Thomas S, Petovar B, Finsgar MA (2017) A flexible, disposable hydrogen peroxide sensor on graphene nanoplatelet-coated cellulose. *Curr Anal Chem* 13(6):480–487. <https://doi.org/10.2174/1573411013666170427121958>
- Lay M, Pèlach M, Pellicer N, Tarrés JA, Bun KN, Vilaseca F (2017) Smart nanopaper based on cellulose nanofibers with hybrid PEDOT:PSS/polypyrrole for energy storage devices. *Carbohydr Polym* 165:86–95. <https://doi.org/10.1016/j.carbpol.2017.02.043>
- Li W, Yang Y, Sha J, Zhou J, Qin C, Wang S (2018) The influence of mechanical refining treatments on the rheosedimentation properties of bleached softwood pulp suspensions. *Cellulose* 25(6):3609–3618. <https://doi.org/10.1007/s10570-018-1808-1>
- Liao WH, Yang SY, Hsiao ST, Wang YS, Li SM, Ma CC, Tien HW, Zeng SJ (2014) Effect of octa(aminophenyl) polyhedral oligomeric silsesquioxane functionalized graphene oxide on the mechanical and dielectric properties of polyimide composites. *ACS Appl Mater Interfaces* 6(18):15802–15812. <https://doi.org/10.1021/am504342j>
- Lunkenheimer P, Bobnar V, Bobnar V, Pronin AV, Ritus AI, Volkov AA, Loidl A (2002) Origin of apparent colossal dielectric constants. *Phys Rev B Condens Matter Mater Phys* 66(5):052105. <https://doi.org/10.1103/PhysRevB.66.052105>
- Madusanka N, Shivareddy SG, Eddleston MD, Hiralal P, Oliver RA, Amaratunga GA (2017) Dielectric behaviour of montmorillonite/cyanoethylated cellulose nanocomposites. *Carbohydr Polym* 172:315–321. <https://doi.org/10.1016/j.carbpol.2017.05.057>
- Marcano DC, Kosynkin DV, Berlin JM, Sinitskii A, Sun Z, Slesarev A, Alemany LB, Lu W, Tour JM (2010) Improved synthesis of graphene oxide. *ACS Nano* 4(8):4806–4814. <https://doi.org/10.1021/nn1006368>
- Mohiuddin M, Sadasivuni KK, Mun S, Kim J (2015) Flexible cellulose acetate/graphene blueprints for vibrotactile actuator. *RSC Adv* 5(43):34432–34438. <https://doi.org/10.1039/C5RA03043A>
- Ning N, Ma Q, Liu S, Tian M, Zhang L, Nishi T (2015) Tailoring dielectric and actuated properties of elastomer composites by bioinspired poly(dopamine) encapsulated graphene oxide. *ACS Appl Mater Interfaces* 7(20):10755–10762. <https://doi.org/10.1021/acsami.5b00808>
- Nishiyama Y (2009) Structure and properties of the cellulose microfibril. *J Wood Sci* 55(4):241–249. <https://doi.org/10.1007/s10086-009-1029-1>
- Nyangiwe NN, Khenfouch M, Thema FT, Nukwa K, Kotsedi L, Maaza M (2015) Free-green synthesis and dynamics of reduced graphene sheets via sun light irradiation. *Graphene* 4(03):54. <https://doi.org/10.4236/graphene.2015.43006>
- Pei S, Cheng H-M (2012) The reduction of graphene oxide. *Carbon N Y* 50(9):3210–3228. <https://doi.org/10.1016/j.carbon.2011.11.010>
- Pottathara YB, Bobnar V, Finšgar M, Grohens Y, Thomas S, Kokol V (2018) Cellulose nanofibrils-reduced graphene oxide xerogels and cryogels for dielectric and electrochemical storage applications. *Polymer* 147:260–270. <https://doi.org/10.1016/j.polymer.2018.06.005>
- Pottathara YB, Narwade VN, Bogle KA, Kokol V (2019) TEMPO-oxidized cellulose nanofibrils–graphene oxide composite films with improved dye adsorption properties. *Polym Bull.* <https://doi.org/10.1007/s00289-019-03077-3>

- Pottathara YB, Thomas S, Kalarikkal N, Grießer T, Grohens Y, Bobnar V, Finšgar M, Kokol V, Kargl R (2019b) UV-Induced reduction of graphene oxide in cellulose nanofibril composites. *New J Chem* 43(2):681–688. <https://doi.org/10.1039/C8NJ03563F>
- Poyraz B, Tozluoğlu A, Candan Z, Demir A, Yavuz M (2017) Influence of PVA and silica on chemical, thermo-mechanical and electrical properties of Celluclast-treated nanofibrillated cellulose composites. *Int J Biol Macromol* 104:384–392. <https://doi.org/10.1016/j.ijbiomac.2017.06.018>
- Sadasivuni KK, Kafy A, Kim H-C, Ko HU, Mun S, Kim J (2015) Reduced graphene oxide filled cellulose films for flexible temperature sensor application. *Synth Met* 206:154–161. <https://doi.org/10.1016/j.synthmet.2015.05.018>
- Saito T, Nishiyama Y, Pataux JL, Vignon M, Isogai A (2006) Homogeneous suspensions of individualized microfibrils from TEMPO-catalyzed oxidation of native cellulose. *Biomacromolecules* 7(6):1687–1691. <https://doi.org/10.1021/bm060154s>
- Saito T, Kimura S, Nishiyama Y, Isogai A (2007) Cellulose nanofibers prepared by TEMPO-mediated oxidation of native cellulose. *Biomacromolecules* 8(8):2485–2491. <https://doi.org/10.1021/bm0703970>
- Saito T, Kuramae R, Wohler J, Berglund LA, Isogai A (2013) An ultrastrong nanofibrillar biomaterial: the strength of single cellulose nanofibrils revealed via sonication-induced fragmentation. *Biomacromolecules* 14(1):248–253. <https://doi.org/10.1021/bm301674e>
- Shi Z, Gao H, Feng J, Ding B, Cao X, Kuga S, Wang Y, Zhang L, Cai J (2014) In situ synthesis of robust conductive cellulose/polypyrrole composite aerogels and their potential application in nerve regeneration. *Angew Chem Int Ed* 53(21):5380–5384. <https://doi.org/10.1002/anie.201402751>
- Shi K, Zou H, Sun B, Jiang P, He J, Huang X (2020) Dielectric modulated cellulose paper/PDMS-based triboelectric nanogenerators for wireless transmission and electropolymerization applications. *Adv Funct Mater* 30(4):1904536. <https://doi.org/10.1002/adfm.201904536>
- Tao J, Cao SA (2020) Flexible high dielectric thin films based on cellulose nanofibrils and acid oxidized multi-walled carbon nanotubes. *RSC Adv* 10(18):10799–10805. <https://doi.org/10.1039/c9ra10915c>
- Tao J, Cao SA, Liu W, Deng Y (2019) Facile preparation of high dielectric flexible films based on titanium dioxide and cellulose nanofibrils. *Cellulose* 26(10):6087–6098. <https://doi.org/10.1007/s10570-019-02495-w>
- Tao J, Cao SA, Feng R, Deng Y (2020) High dielectric thin films based on barium titanate and cellulose nanofibrils. *RSC Adv* 10(10):5758–5765. <https://doi.org/10.1039/C9RA10916A>
- Tong W, Zhang Y, Zhang Q, Luan X, Duan Y, Pan S, Lv F, An Q (2015) Achieving significantly enhanced dielectric performance of reduced graphene oxide/polymer composite by covalent modification of graphene oxide surface. *Carbon N Y* 94:590–598. <https://doi.org/10.1016/j.carbon.2015.07.005>
- Wang F, Wang M, Shao Z (2018) Dispersion of reduced graphene oxide with montmorillonite for enhancing dielectric properties and thermal stability of cyanoethyl cellulose nanocomposites. *Cellulose* 25(12):7143–7152. <https://doi.org/10.1007/s10570-018-2049-z>
- Wu C, Huang X, Wu X, Xie L, Yang K, Jiang P (2013) Graphene oxide-encapsulated carbon nanotube hybrids for high dielectric performance nanocomposites with enhanced energy storage density. *Nanoscale* 5(9):3847–3855. <https://doi.org/10.1039/c3nr00625e>
- Yang C, Li D (2015) Flexible and foldable supercapacitor electrodes from the porous 3D network of cellulose nanofibers, carbon nanotubes and polyaniline. *Mater Lett* 155:78–81. <https://doi.org/10.1016/j.matlet.2015.04.096>
- Yang Q, Saito T, Berglund LA, Isogai A (2015) Cellulose nanofibrils improve the properties of all-cellulose composites by the nano-reinforcement mechanism and nanofibril-induced crystallization. *Nanoscale* 7(42):17957–17963. <https://doi.org/10.1039/c5nr05511c>
- Yang Q, Zhang C, Shi Z, Wang J, Xiong C, Saito T, Isogai A (2018) Luminescent and transparent nanocellulose films containing europium carboxylate groups as flexible dielectric materials. *ACS Appl Nano Mater* 1(9):4972–4979. <https://doi.org/10.1021/acsnm.8b01112>
- Yin Y, Zhang C, Yu W, Kang G, Yang Q, Shi Z, Xiong C (2020) Transparent and flexible cellulose dielectric films with high breakdown strength and energy density. *Energy Storage Mater* 26:105–111. <https://doi.org/10.1016/j.ensm.2019.12.034>
- Yuan JK, Yao SH, Dang ZM, Sylvestre A, Genestoux M, Bai J (2011) Giant dielectric permittivity nanocomposites: Realizing true potential of pristine carbon nanotubes in polyvinylidene fluoride matrix through an enhanced interfacial interaction. *J Phys Chem C* 115(13):5515–5521. <https://doi.org/10.1021/jp1117163>
- Yuwawech K, Woothikanokkhan J, Tanpichai S (2015) Enhancement of thermal, mechanical and barrier properties of EVA solar cell encapsulating films by reinforcing with esterified cellulose nanofibres. *Polym Test* 48:12–22. <https://doi.org/10.1016/j.polymertesting.2015.09.007>
- Zeng X, Deng L, Yao Y, Sun R, Xu J, Wong CP (2016) Flexible dielectric papers based on biodegradable cellulose nanofibers and carbon nanotubes for dielectric energy storage. *J Mater Chem C* 4(25):6037–6044. <https://doi.org/10.1039/c6tc01501h>
- Zhang H, Wang Z, Zhang ZN, Wu J, Zhang J, He JS (2007) Regenerated-cellulose/multiwalled-carbon-nanotube composite fibers with enhanced mechanical properties prepared with the ionic liquid 1-allyl-3-methylimidazolium chloride. *Adv Mater* 19(5):698–704. <https://doi.org/10.1002/adma.200600442>
- Zhang C, Yin Y, Yang Q, Shi Z, Hu GH, Xiong C (2019) Flexible cellulose/BaTiO₃ nanocomposites with high energy density for film dielectric capacitor. *ACS Sustain Chem Eng* 7(12):10641–10648. <https://doi.org/10.1021/acssuschemeng.9b01302>
- Zhao Y, Dang W, Si L, Lu Z (2019) Enhanced mechanical and dielectric properties of Aramid fiber/Mica-nanofibrillated cellulose composite paper with biomimetic multilayered structure. *Cellulose* 26(3):2035–2046. <https://doi.org/10.1007/s10570-018-2170-z>

Publisher's note Springer Nature remains neutral with regard to jurisdictional claims in published maps and institutional affiliations.